The Parameter Averaging Technique in Finite-Difference Modeling of Elastic Waves in Combined Structures with Solid, Fluid and Porous Subregions

Wei Guan* and Hengshan Hu

Department of Astronautics and Mechanics, Harbin Institute of Technology, Postbox 344, 92 West Dazhi Street, Harbin 150001, China.

Abstract. To finite-difference model elastic wave propagation in a combined structure with solid, fluid and porous subregions, a set of modified Biot's equations are used, which can be reduced to the governing equations in solids, fluids as well as fluid-saturated porous media. Based on the modified Biot's equations, the field quantities are finite-difference discretized into unified forms in the whole structure, including those on any interface between the solid, fluid and porous subregions. For the discrete equations on interfaces, however, the harmonic mean of shear modulus and the arithmetic mean of the other parameters on both sides of the interfaces are used. These parameter averaging equations are validated by deriving from the continuity conditions on the interfaces. As an example of using the parameter averaging technique, a 2-D finite-difference scheme with a velocity-stress staggered grid in cylindrical coordinates is implemented to simulate the acoustic logs in porous formations. The finite-difference simulations of the acoustic logging in a homogeneous formation agree well with those obtained by the analytical method. The acoustic logs with mud cakes clinging to the borehole well are simulated for investigating the effect of mud cake on the acoustic logs. The acoustic logs with a varying radius borehole embedded in a horizontally stratified formation are also simulated by using the proposed finite-difference scheme.

AMS subject classifications: 76M20, 65M06, 76S05, 35L05, 86A15

Key words: Finite-difference, wave equation, porous medium, acoustic logging, numerical simulation.

1 Introduction

In petroleum exploration a reservoir can be described as a fluid-saturated porous medium, which consists of solid frame and pore fluid. Studies of elastic wave propagation in

---

*Corresponding author. *Email addresses:* `gwllzh@tom.com` (W. Guan), `wave_hu@yahoo.com` (H. Hu)

such a medium become increasingly important to obtain more detailed reservoir information and monitor pore fluid flow. Biot [3–5] put forward the theory of wave propagation in a homogeneous fluid-saturated porous medium allowed for the interaction between the solid frame and the pore fluid. An important achievement of Biot's theory was the prediction of the second kind compressional wave in one-fluid-saturated porous media [19]. After the establishment of Biot's theory, many investigators have used it to study the wave propagation in porous formations. For example, Deresiewicz and Skalak [10] provided the boundary conditions on an interface between two different porous media. Rosenbaum [22] and Schmitt [23] calculated the monopole acoustic logs in homogeneous porous formations by applying the real-axis integration (RAI) method. Norris [18] derived the analytical fundamental solutions in the form of Green's function for a point force applied in an unbounded poroelastic medium. Based on the Green's function, the wave propagation in horizontally stratified porous formations was simulated by Boutin et al. [7]. However, analytical solutions for Biot's equations are in general impossible for arbitrary heterogeneous porous formations. In order to simulate poroelastic wave propagation in complex cases, finite-difference methods were applied (e.g., Zhu and McMechan [31], Dai et al. [9], Zhang [29], Zeng et al. [30], Song et al. [24], and Masson et al. [16]).

In a finite-difference algorithm, the heterogeneous formation is divided into discrete grid, so that the field quantities and governing equations for wave propagation are discretized to the grid. Due to the parameter discontinuities across an interface between different homogeneous media, the discrete equations for field quantities on the interface are commonly different from those for the ones in homogeneous media. Masson et al. [16] directly formulated the discrete equations on an interface between two different porous media by replacing the parameters in the discrete equations in homogeneous media with the averages of the two porous media. This parameter averaging technique is originated from the finite-difference modeling of electromagnetic waves. It has been derived that the discrete equations with average parameters comply with the continuity conditions of the electromagnetic fields on the interface [14]. For the finite-difference modeling of elastic wave propagation, however, the parameter averaging technique has not been validated by derivation in literature. Thus in previous papers the parameters in the discrete equations on interfaces were averaged by different manners. For example, the harmonic mean of shear modulus was used in Masson et al. [16] and in Song [25], while the arithmetic mean was used in Mittet [17]. Moreover, the parameter averaging technique was used only for interfaces between two media of the same type, such as porous-porous and solid-solid interfaces. If the wave equations on both sides of the interfaces are in different forms, such as for a fluid-porous interface, the parameter averaging technique cannot be used. Dong et al. [11] and Guan et al. [13] respectively formulated the discrete equations on fluid-porous interface by solving the linear equations based on the continuity conditions across the interface. Nevertheless, their method complicates the algorithm implementation because of the additional deriving on various interfaces at different locations, and is inconvenient for the intersection between three different media.

In this paper, the validity of the parameter averaging technique is determined. We derive the discrete equations on an interface between two media of the same type by using the discrete equations in the two homogeneous porous media and the continuity conditions of the field quantities across the interface. These discrete equations on the interface have the same forms as those in homogeneous media, but use the harmonic mean of shear modulus and the arithmetic mean of the other parameters. Furthermore, using a set of modified Biot's equations to express elastic wave propagation in solid, fluid as well as porous media, we extend the parameter averaging technique for interfaces between different kinds of media, such as a fluid-porous interface. Based on the modified Biot's equations and the parameter averaging technique, a 2-D finite-difference time-domain scheme is presented for simulating elastic wave propagation in combined structures with solid, fluid and porous subregions. In this scheme, the finite-difference discrete equations are formulated in unified forms in the whole computational region including those on any interface.

The paper is organized as follows: in Section 2, we briefly review Biot's equations which govern elastic wave propagation in homogeneous fluid-saturated porous media. In Section 3, we derive the discrete equations with average parameters on an interface between two different porous media. In Section 4, Biot's equations are modified to govern elastic wave propagation in solid, fluid as well as porous media. Based on the general equations, the parameter averaging technique is applied for any interface between solid, fluid and porous media. In Section 5, we discretize the modified Biot's equations and implement the 2-D finite-difference scheme for the modeling of elastic wave propagation in combined structures with solid, fluid and porous subregions. The perfectly matched layer absorbing boundary condition without splitting the fields is applied to eliminate the spurious reflections from the artificial boundaries of the computational region. By using the proposed scheme the monopole acoustic logs in fluid-saturated porous formations are simulated in Section 6. The finite-difference modeled acoustic logs in a homogeneous porous formation are compared with the analytical results obtained by the RAI method. The effect of mud cake on acoustic logs is investigated by calculating the waveforms of the acoustic logging with a mud cake clinging to the borehole wall. Simulations of the acoustic logs in horizontally stratified porous formations are also given.

2   Biot's equations

Biot [3–5] studied the interaction between the solid framework strain and the pore fluid filtration when elastic waves propagate through a fluid-saturated porous medium and established a set of governing equations. In his works, a generalized Darcy's law is proposed to allow for both the flow due to the induced pressure gradient and the flow created by the acceleration of the solid framework which is the frame of reference for the relative fluid flow. Assuming an $e^{-i\omega t}$ time dependence, the generalized Darcy law is

written in the frequency domain as (e.g., Masson et al. [16])

$$\mathbf{v}_\omega = \frac{\kappa(\omega)}{\eta}(-\nabla p + i\omega\rho_f\mathbf{v}_u), \tag{2.1}$$

where $\mathbf{v}_u$ is the solid phase velocity, $\mathbf{v}_\omega$ is the velocity of the relative flow between the pore fluid and the solid phase, which can be expressed as $\mathbf{v}_\omega = \phi(\mathbf{v}_f - \mathbf{v}_u)$, ϕ is the porosity and $\mathbf{v}_f$ is the pore fluid velocity, p is the pore fluid pressure, ρ_f and η are the density and the viscosity of the pore fluid, respectively, $\kappa(\omega)$ is the dynamic permeability function defined by Johnson et al. [15], which has the following form

$$\kappa(\omega) = \kappa_0 \left[\left(1 - \frac{4i\omega}{m\omega_c}\right)^{\frac{1}{2}} - i\frac{\omega}{\omega_c} \right]^{-1}. \tag{2.2}$$

Here κ_0 is the Darcy permeability, the term $(1 - 4i\omega/m\omega_c)^{1/2}$ dependent on frequency denotes the frequency correction function for the viscous force term in Biot's equations, and the critical frequency $\omega_c = \phi\eta/\alpha_\infty\rho_f\kappa_0$ separates the low-frequency viscous flow from the high-frequency inertial flow, where α_∞ is the tortuosity, $m = \phi\Lambda^2/\alpha_\infty\kappa_0$ is a dimensionless parameter, Λ is the weighted volume-to-surface radio.

In order to finite-difference discretize (2.1) in the time domain, Taylor expansion is applied to the term $(1 - 4i\omega/m\omega_c)^{1/2}$ in (2.2) under the condition that $|4\omega/m\omega_c| < 1$, one obtains

$$\left(1 - \frac{4i\omega}{m\omega_c}\right)^{\frac{1}{2}} = 1 - \frac{1}{2}\left(\frac{4i\omega}{m\omega_c}\right) - \frac{1}{8}\left(\frac{4i\omega}{m\omega_c}\right)^{\frac{1}{2}} + \mathcal{O}\left(\frac{\omega^3}{\omega_c^3}\right). \tag{2.3}$$

For a typical sandstone (where $m \approx 8$) and $\omega < 2\omega_c$, the third term in the right hand side of (2.3) is a small quantity of higher order and can be ignored, thus the term $(1 - 4i\omega/m\omega_c)^{1/2}$ is approximated as $1 - 2i\omega/m\omega_c$. Then (2.1) is approximately rewritten in the time domain as

$$\rho_f\frac{\partial\mathbf{v}_u}{\partial t} + C_1\mathbf{v}_\omega + C_2\frac{\partial\mathbf{v}_\omega}{\partial t} = -\nabla p, \tag{2.4}$$

where $C_1 = \eta/\kappa_0$ and $C_2 = (1 + 2m^{-1})\alpha_\infty\rho_f/\phi$.

The remaining Biot's equations with respect to velocities and stresses in the time domain are given by

$$\frac{\partial\boldsymbol{\tau}}{\partial t} = (H - 2\mu)(\nabla\cdot\mathbf{v}_u)\mathbf{I} + C(\nabla\cdot\mathbf{v}_\omega)\mathbf{I} + \mu(\nabla\mathbf{v}_u + \mathbf{v}_u\nabla), \tag{2.5a}$$

$$\frac{\partial p}{\partial t} = -(C\nabla\cdot\mathbf{v}_u + M\nabla\cdot\mathbf{v}_\omega), \tag{2.5b}$$

$$\rho\frac{\partial\mathbf{v}_u}{\partial t} + \rho_f\frac{\partial\mathbf{v}_\omega}{\partial t} = \nabla\cdot\boldsymbol{\tau}, \tag{2.5c}$$

where τ is the bulk stress tensor, **I** is the identity tensor, ρ is the density of the porous medium, which is expressed by the solid grain density ρ_s and the pore fluid density ρ_f as $\rho = (1-\phi)\rho_s + \phi\rho_f$, μ is the shear modulus, H, C and M are porous medium moduli defined by Biot [5], which are written as

$$M = \frac{K_f K_s}{\phi K_s + (\alpha - \phi)K_f}, \tag{2.6a}$$

$$C = M\alpha, \tag{2.6b}$$

$$H = K_u + \frac{4\mu}{3}. \tag{2.6c}$$

Here K_s and K_f are the bulk moduli of the solid grain and pore fluid, respectively, K_u is the undrained bulk modulus, i.e., the bulk modulus of the fluid-saturated porous medium, $\alpha = 1 - K_d/K_s$ is the Biot-Willis constant [6], where K_d is the drained bulk modulus, i.e., the bulk modulus of the solid framework, and the relation $K_u = \alpha^2 M + K_d$ is known as the Gassmann equation [12].

3 Parameter averaging technique

An axisymmetric cylindrical coordinate system (r,θ,z), in which all field components are independent of θ, is used as an example for deriving the finite-difference discrete equations on an interface between two different porous media. The velocity and stress fields for Biot's poroelastic waves in the 2-D cylindrical coordinates are discretized by using a staggered finite-difference grid (Randall [20], Song et al. [24]), as shown in Fig. 1. The staggered grid is composed of rectangular cells formed by solid grid lines. The integers j and k denote the indices of the solid lines arrayed in the r and z directions, respectively. The normal stresses τ_{rr}, $\tau_{\theta\theta}$ and τ_{zz} are located at the center of cells, while the shear stress τ_{rz} is located at the corners. All the velocity components are centered on the cell sides.

The medium parameters are set to be constant within a cell, thus the interfaces can be only located along the solid grid lines between different cells. In this case, according
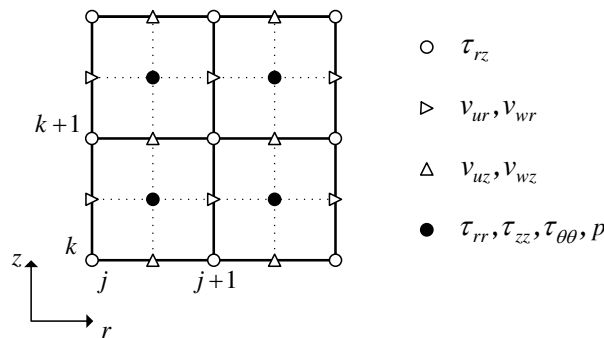

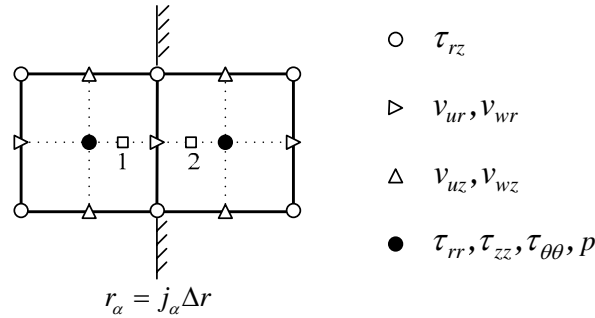Figure 1: Velocity-stress finite-difference staggered grid in axisymmetric cylindrical coordinates.

Figure 2: Schematic of the interface between two different porous media.

to the boundary conditions given by Deresiewicz and Skalak [10], the quantities v_{ur}, $v_{\omega r}$ and τ_{rz} located on an interface perpendicular to the r direction are continuous across the interface and the quantities v_{uz}, $v_{\omega z}$ and τ_{rz} located on an interface perpendicular to the z direction are also continuous across the interface. Note that if the locations of field quantities on the cells are changed (for example the cells are formed by the dotted lines in Fig. 1), the quantity $\tau_{\theta\theta}$ allowed to be discontinuous will be on an interface. Due to the discontinuity, the values of $\tau_{\theta\theta}$ may be different on the left and right sides of the interface. Representing the two different values by a single variable in a finite-difference scheme will lead to incorrect simulations.

Shown in Fig. 2 is an interface between two different porous media at $r_\alpha = j_\alpha \Delta r$, where Δr is the cell size in the r direction. It is seen that the velocities v_{ur}, $v_{\omega r}$ and the shear stress τ_{rz} are located on this interface. To calculate these three field quantities, one has to use the following component equations in the 2-D cylindrical coordinates (e.g., Berryman and Pride [2]),

$$\rho\frac{\partial v_{ur}}{\partial t}+\rho_f\frac{\partial v_{\omega r}}{\partial t}=\frac{\partial \tau_{rr}}{\partial r}+\frac{1}{r}\tau_{rr}-\frac{1}{r}\tau_{\theta\theta}+\frac{\partial \tau_{rz}}{\partial z}, \tag{3.1a}$$

$$\rho_f\frac{\partial v_{ur}}{\partial t}+C_1 v_{\omega r}+C_2\frac{\partial v_{\omega r}}{\partial t}=-\frac{\partial p}{\partial r}, \tag{3.1b}$$

$$\frac{\partial \tau_{rz}}{\partial t}=\mu\left(\frac{\partial v_{uz}}{\partial r}+\frac{\partial v_{ur}}{\partial z}\right). \tag{3.1c}$$

For the grid points in a homogeneous porous medium ($r=j\Delta r$, $j \neq j_\alpha$), the partial differential equations (3.1a)-(3.1c) can be finite-difference discretized directly. For example, the discrete expression of (3.1a) is written as

$$\rho_j\left(\frac{\partial v_{ur}}{\partial t}\right)_j+\rho_{fj}\left(\frac{\partial v_{\omega r}}{\partial t}\right)_j=\left(\frac{\partial \tau_{rr}}{\partial r}\right)_j+\frac{1}{r}\frac{(\tau_{rr}-\tau_{\theta\theta})_{j+\frac{1}{2}}+(\tau_{rr}-\tau_{\theta\theta})_{j-\frac{1}{2}}}{2}+\left(\frac{\partial \tau_{rz}}{\partial z}\right)_j, \tag{3.2}$$

where ρ_j and ρ_{fj} are the densities of the homogeneous porous medium at $r=j\Delta r$, $j\neq j_\alpha$. Because τ_{rr} and $\tau_{\theta\theta}$ are not assigned at $r=j\Delta r$, their values are approximated as

$$(\tau_{rr})_j=\frac{1}{2}\left((\tau_{rr})_{j-\frac{1}{2}}+(\tau_{rr})_{j+\frac{1}{2}}\right) \quad \text{and} \quad (\tau_{\theta\theta})_j=\frac{1}{2}\left((\tau_{\theta\theta})_{j-\frac{1}{2}}+(\tau_{\theta\theta})_{j+\frac{1}{2}}\right)$$

in (3.2).

Due to the break of medium parameters on the interface, (3.2) is invalid for the grid points at $r_\alpha = j_\alpha \Delta r$. In order to formulate the discrete equations on the interface, we select two space points (numbered "1" and "2" in Fig. 2) that respectively close to the left and right sides of the interface. For the two points that in homogeneous media, (3.1a) is discretized as

$$\rho_1 \left(\frac{\partial v_{ur}}{\partial t}\right)_1 + \rho_{f1} \left(\frac{\partial v_{\omega r}}{\partial t}\right)_1 = \left(\frac{\partial \tau_{rr}}{\partial r}\right)_1 + \left(\frac{1}{r}\tau_{rr}\right)_1 - \left(\frac{1}{r}\tau_{\theta\theta}\right)_1 + \left(\frac{\partial \tau_{rz}}{\partial z}\right)_1, \qquad (3.3a)$$

$$\rho_2 \left(\frac{\partial v_{ur}}{\partial t}\right)_2 + \rho_{f2} \left(\frac{\partial v_{\omega r}}{\partial t}\right)_2 = \left(\frac{\partial \tau_{rr}}{\partial r}\right)_2 + \left(\frac{1}{r}\tau_{rr}\right)_2 - \left(\frac{1}{r}\tau_{\theta\theta}\right)_2 + \left(\frac{\partial \tau_{rz}}{\partial z}\right)_2, \qquad (3.3b)$$

where ρ_1 and ρ_{f1} denote the densities of the porous medium and the pore fluid at the location "1", while ρ_2 and ρ_{f2} denote those at the location "2". Using the continuities of v_{ur} and $v_{\omega r}$ on the interface, we obtain $(v_{ur})_1 \approx (v_{ur})_2 \approx (v_{ur})_{r_\alpha}$ and $(v_{\omega r})_1 \approx (v_{\omega r})_2 \approx (v_{\omega r})_{r_\alpha}$. Introducing the parameters $\rho_{AM} = (\rho_1 + \rho_2)/2$ and $\rho_{f\_AM} = (\rho_{f1} + \rho_{f2})/2$, yields

$$\rho_1 \left(\frac{\partial v_{ur}}{\partial t}\right)_1 + \rho_2 \left(\frac{\partial v_{ur}}{\partial t}\right)_2 = 2\rho_{AM} \left(\frac{v_{ur}}{\partial t}\right)_{r_\alpha}, \qquad (3.4a)$$

$$\rho_{f1} \left(\frac{\partial v_{\omega r}}{\partial t}\right)_1 + \rho_{f2} \left(\frac{\partial v_{\omega r}}{\partial t}\right)_2 = 2\rho_{f\_AM} \left(\frac{v_{\omega r}}{\partial t}\right)_{r_\alpha}. \qquad (3.4b)$$

The continuity of τ_{rz} on the interface leads to an approximation of $(\tau_{rz})_1 \approx (\tau_{rz})_2 \approx (\tau_{rz})_{r_\alpha}$. Then the following equation is obtained

$$\left(\frac{\partial \tau_{rz}}{\partial z}\right)_1 + \left(\frac{\partial \tau_{rz}}{\partial z}\right)_2 = 2\left(\frac{\partial \tau_{rz}}{\partial z}\right)_{r_\alpha}. \qquad (3.5)$$

Using the continuity of the stress component τ_{rr} on the interface gives

$$\left(\frac{\partial \tau_{rr}}{\partial r}\right)_1 + \left(\frac{\partial \tau_{rr}}{\partial r}\right)_2 = \left(\frac{\Delta r}{2}\right)^{-1} \left[\tau_{rr}\left(r_\alpha + \frac{1}{2}, k + \frac{1}{2}\right) - \tau_{rr}\left(r_\alpha - \frac{1}{2}, k + \frac{1}{2}\right)\right] = 2\left(\frac{\partial \tau_{rr}}{\partial r}\right)_{r_\alpha}. \quad (3.6)$$

Then adding (3.3a) and (3.3b) together, using (3.4a)-(3.6), and introducing the common finite-difference approximations $(\tau_{rr})_1 \approx (\tau_{rr})_{r_\alpha - 1/2}$, $(\tau_{rr})_2 \approx (\tau_{rr})_{r_\alpha + 1/2}$, $(\tau_{\theta\theta})_1 \approx (\tau_{\theta\theta})_{r_\alpha - 1/2}$ and $(\tau_{\theta\theta})_2 \approx (\tau_{\theta\theta})_{r_\alpha + 1/2}$, the discrete expression of (3.1a) on the interface at $r_\alpha = j_\alpha \Delta r$ is obtained

$$\rho_{AM} \left(\frac{\partial v_{ur}}{\partial t}\right)_{r_\alpha} + \rho_{f\_AM} \left(\frac{\partial v_{\omega r}}{\partial t}\right)_{r_\alpha}$$
$$= \left(\frac{\partial \tau_{rr}}{\partial r}\right)_{r_\alpha} + \frac{1}{r}\frac{(\tau_{rr} - \tau_{\theta\theta})_{r_\alpha + \frac{1}{2}} + (\tau_{rr} - \tau_{\theta\theta})_{r_\alpha - \frac{1}{2}}}{2} + \left(\frac{\partial \tau_{rz}}{\partial z}\right)_{r_\alpha}. \qquad (3.7)$$

It is seen that (3.7) has the same form as (3.2) in the homogeneous medium, but the parameters ρ_{AM} and ρ_{f_AM} are used instead, which are the arithmetic means of those in the homogeneous media on both sides of the interface.

Adopting a similar way to the derivation of (3.7), the discrete expression of (3.1b) on the interface is given by

$$\rho_{f\_AM}\left(\frac{\partial v_{ur}}{\partial t}\right)_{r_\alpha} + C_{1\_AM}(v_{\omega r})_{r_\alpha} + C_{2\_AM}\left(\frac{\partial v_{\omega r}}{\partial t}\right)_{r_\alpha} = -\left(\frac{\partial p}{\partial r}\right)_{r_\alpha}, \tag{3.8}$$

where $C_{1\_AM} = (C_{11}+C_{12})/2$, $C_{2\_AM} = (C_{21}+C_{22})/2$, C_{1q} and C_{2q} ($q=1,2$), denote the parameters C_1 and C_2 of the porous media on both sides of the interface.

To discretize (3.1c) on the interface, shifting the shear modulus μ to the left hand and using the continuities of τ_{rz}, v_{uz} and v_{ur} on the interface gives

$$\left(\frac{1}{\mu}\right)_{AM}\left(\frac{\partial \tau_{rz}}{\partial t}\right)_{r_\alpha} = \left(\frac{\partial v_{uz}}{\partial r} + \frac{\partial v_{ur}}{\partial z}\right)_{r_\alpha}. \tag{3.9}$$

As the shear stress is assigned at the corners of a cell, $(1/\mu)_{AM}$ in (3.9) is calculated by the arithmetic mean of $1/\mu$ in the four cells neighboring the shear stress position, which is formulated as

$$\left(\frac{1}{\mu}\right)_{AM} = \frac{1}{4}\sum_{q=1}^{4}\frac{1}{\mu_q}.$$

Shifting the parameter $(1/\mu)_{AM}$ into the right hand of (3.9) yields

$$\left(\frac{\partial \tau_{rz}}{\partial t}\right)_{r_\alpha} = \mu_{HM}\left(\frac{\partial v_{uz}}{\partial r} + \frac{\partial v_{ur}}{\partial z}\right)_{r_\alpha}, \tag{3.10}$$

where μ_{HM} is the reciprocal of $(1/\mu)_{AM}$, i.e., the harmonic mean of μ.

It is shown by (3.7), (3.8) and (3.10) that the discrete equations on a porous-porous interface can be formulated directly in the forms of those in a homogeneous medium, if the harmonic mean of shear modulus μ and the arithmetic mean of the other parameters are used. Although the above discrete equations with average parameters are derived in the 2-D coordinates, the parameter averaging technique is available for 3-D finite-difference modeling problems because the field quantity in a 3-D finite-difference grid is still calculated by using its adjacent field quantities on the 2-D plane.

4 General equations for solid, fluid and porous media

From the above derivation it is seen that the governing equations on both sides of the interface must be in the same form when using the parameter averaging technique. For wave propagation in a combined structure with solid, fluid and porous subregions, there are interfaces between distinct kinds of media. For example, in the acoustic logging in porous formations, the borehole wall is a fluid-porous interface between the borehole fluid and the porous formation. If there is a mud cake that regarded as a solid medium clinging to the borehole wall, the solid-fluid and solid-porous interfaces are also exist. On both sides of these interfaces between solid, fluid and porous media, the governing

equations have different forms. In order to extend the parameter averaging technique for any kind of interface, we will use a set of general equations to describe elastic wave propagation in solid, fluid as well as porous media.

Biot's equations governing elastic wave propagation in fluid-saturated porous media can be reduced to the equations for solids and fluids by setting the limits of certain field quantities and material parameters. A porous medium whose pore spaces are filled with solid grain corresponds to an elastic solid. In this limiting case, the field quantities and parameters in Biot's equations change to $\phi = 0$, $K_d = K_s = K_f = K_{ms}$, $\mu = \mu_{ms}$, $\alpha = 0$, $M = \infty$, $C = K_{ms}$, $H = K_{ms} + 4\mu_{ms}/3$, $\rho_f = \rho = \rho_{ms}$, $\boldsymbol{\tau} = \boldsymbol{\tau}_{ms}$, $\mathbf{v}_u = \mathbf{v}_f = \mathbf{v}_{ms}$, and $\mathbf{v}_\omega = 0$, thus (2.5a) and (2.5c) are reduced to the basic Newton's motion law and continuity equation of the stress and velocity fields in the solid, i.e.,

$$\frac{\partial \boldsymbol{\tau}_{ms}}{\partial t} = \lambda(\nabla \cdot \mathbf{v}_{ms})\mathbf{I} + \mu_{ms}(\nabla \mathbf{v}_{ms} + \mathbf{v}_{ms}\nabla), \tag{4.1a}$$

$$\rho_{ms}\frac{\partial \mathbf{v}_{ms}}{\partial t} = \nabla \cdot \boldsymbol{\tau}_{ms}, \tag{4.1b}$$

where $\lambda = K_{ms} - 2\mu_{ms}/3$, the variables with subscript "ms" denote the stress, velocity, or material parameters in the solid.

A porous medium whose solid frame is replaced by the pore fluid corresponds to a fluid. In this limiting case, the field quantities and parameters in Biot's equations become $\phi = 1$, $K_d = 0$, $K_s = K_f = K_{mf}$, $\mu = 0$, $\alpha = 1$, $C = M = H = K_{mf}$, $\rho_f = \rho = \rho_{mf}$, $\boldsymbol{\tau} = -p_{mf}\mathbf{I}$, $\mathbf{v}_f = \mathbf{v}_u = \mathbf{v}_{mf}$, and $\mathbf{v}_\omega = 0$, hence (2.5a) and (2.5c) are reduced to the governing equations in the fluid, i.e.,

$$\frac{\partial p_{mf}}{\partial t} = -\rho_{mf}v_{mf}^2\nabla \cdot \mathbf{v}_{mf}, \tag{4.2a}$$

$$\rho_{mf}\frac{\partial \mathbf{v}_{mf}}{\partial t} = -\nabla p_{mf}, \tag{4.2b}$$

where the variables with subscript "mf" denote the fluid pressure, velocity, or density.

It is seen that elastic wave propagation in a solid or fluid can be solved by using Biot's equations (2.5a) and (2.5c) in limiting cases. The rest of Biot's equations (2.4) and (2.5b) are not required. The variables $\mathbf{v}_u$ and $\boldsymbol{\tau}$ respectively denote the velocity and stress field of the solid or fluid, while $\mathbf{v}_\omega$ and p are redundant. The variable $\mathbf{v}_\omega$ is directly set as zero when solving (2.5a) and (2.5c), and p is simply set to be the negative value of the mean normal stress after the calculation of $\boldsymbol{\tau}$. For the fluid, the normal stresses in different directions are of the same value and are equal to the negative fluid pressure, while the shear stress components of $\boldsymbol{\tau}$ are zero.

In order to implement the finite-difference scheme of using general equations in solid, fluid and porous media, shifting the second term in the left hand side of (2.5c) to the right hand side and then substituting it into (2.4), Biot's equations (2.4) and (2.5c) are rewritten

as

$$C_1\mathbf{v}_\omega + \left(C_2 - \frac{\rho_f^2}{\rho}\right)\frac{\partial \mathbf{v}_\omega}{\partial t} = -\nabla p - \frac{\rho_f}{\rho}\nabla \cdot \boldsymbol{\tau}, \tag{4.3a}$$

$$\rho\frac{\partial \mathbf{v}_u}{\partial t} = \nabla \cdot \boldsymbol{\tau} - \rho_f\frac{\partial \mathbf{v}_\omega}{\partial t}. \tag{4.3b}$$

The field quantities in solid, fluid as well as porous media can be discretized from the modified Biot's equations composed of (2.5a), (2.5b), (4.3a), and (4.3b). For a staggered finite-difference grid, velocities and stresses are calculated alternately in time. When calculating the velocities, $\mathbf{v}_\omega$ is obtained by solving (4.3a) for a porous medium or it is set as zero for a solid or a fluid. Then the velocity $\mathbf{v}_u$ is determined by substituting the known value of $\mathbf{v}_\omega$ into (4.3b). Compared with using (4.1a) and (4.1b) for the solid or (4.2a) and (4.2b) for the fluid, it does not spend too much CPU time by using the modified Biot's equations. The reason is that only two of the four Biot's equations are actually used in calculation, the redundant field quantities $\mathbf{v}_\omega$ and p need not to be solved from the equations.

The advantage of using the modified Biot's equations in solid, fluid and porous media is that the parameter averaging technique can be extended for solid-fluid, solid-porous and fluid-porous interfaces. For an open pore fluid-porous interface, there is fluid flow across the interface and consequently the relative flow velocity $\mathbf{v}_\omega$ need to be calculated from (4.3a). We give an example to derive the discrete equations of $v_{\omega r}$ on the fluid-porous interface perpendicular to the r direction. Multiplying (3.7) by ρ_{f_AM}/ρ_{AM} and then substituting it into (3.8) yields

$$C_{1\_AM}(v_{\omega r})_{r_\alpha} + \left(C_{2\_AM} - \frac{\rho_{f\_AM}^2}{\rho_{AM}}\right)\left(\frac{\partial v_{\omega r}}{\partial t}\right)_{r_\alpha}$$
$$= -\left(\frac{\partial p}{\partial r}\right)_{r_\alpha} - \frac{\rho_{f\_AM}}{\rho_{AM}}\left[\left(\frac{\partial \tau_{rr}}{\partial r}\right)_{r_\alpha} + \frac{1}{r}\frac{(\tau_{rr}-\tau_{\theta\theta})_{r_\alpha+\frac{1}{2}}+(\tau_{rr}-\tau_{\theta\theta})_{r_\alpha-\frac{1}{2}}}{2} + \left(\frac{\partial \tau_{rz}}{\partial z}\right)_{r_\alpha}\right]. \tag{4.4}$$

The relative flow velocity $v_{\omega r}$ on the fluid-porous interface is discretized by using (4.4) with the arithmetic means of C_1, C_2, ρ_f and ρ on both sides of the interface. In the fluid, both of the parameters ρ_f and ρ are equal to the fluid density, and $C_1 = 0$ and $C_2 = 1$ are calculated by using the limiting values $\kappa_0 = \infty$, $\Lambda = \infty$, $\alpha_\infty = 1$, $\omega_c = 0$, $m = \infty$.

As the relative flow velocity is not possible across a solid-fluid or solid-porous interface, it is set to be zero instead of being calculated from (4.3a). Even though, we briefly analyze the limiting values of C_1, C_2, ρ_f, and ρ in a solid. The parameters ρ_f, and ρ are equal to the solid density, and $C_1 = \infty$, and $C_2 = \infty$ are calculated by using $\kappa_0 = 0$, $\alpha_\infty = \infty$, $\phi/\alpha_\infty\kappa_0 = 0$, and $m = 0$. The values of C_1 and C_2 in the solid make the variable $\mathbf{v}_\omega$ in (4.3a) identically equal to zero, which accords with the physical fact. Similarly, $M = \infty$ in the solid makes $\mathbf{v}_\omega = 0$ in (2.5b). These three input parameters are not used for the simulation of elastic waves in solids, thus they are set as -1.0 in our finite-difference scheme, only to identify them to be the solid parameters.

Based on the general equations and the parameter averaging technique, the velocities and stresses in the whole structure with solid, fluid and porous subregions are finite-difference discretized in the same forms. Hence it takes less CPU time than using the continuity conditions to derive additional equations as in the previous schemes [11, 13] and it has the advantage of easy treatment of complex interfaces, for example, at the intersection of three different media.

5 Finite-difference scheme

For the finite-difference modeling of wave propagation in unbounded structures, as in the case of acoustic logging, the spurious reflections need to be absorbed at the artificial boundaries of the computational region and therefore absorbing boundary conditions must be defined. The perfectly matched layer (PML) absorbing boundary condition with nonsplitting-fields technique (e.g., Roden and Gedney [21], Wang and Tang [28]) is extended to our scheme of the poroelastic wave problem.

To introduce the PML, we rewrite the modified Biot's equations in the complex stretched coordinates (e.g., Chew and Weedon [8], Wang and Tang [28]). The complex coordinate-stretching variable is chosen as $s_q = 1 + \Omega_q/i\omega$ ($q = r, z$), where Ω_q is the stretching function with respect to q. In the complex stretched coordinates, the regular coordinate variable q is replaced by the complex coordinate variable $\tilde{q}$, where

$$\tilde{r} = \int_0^r s_r(r')dr' = r(1 + \overline{\Omega}_r/i\omega), \quad \text{and} \quad \overline{\Omega}_r = \frac{1}{r}\int_0^r \Omega_r(r')dr',$$

and the spatial derivative $\partial/\partial\tilde{q}$ is expressed in terms of the complex coordinate-stretching variable as $\partial/\partial\tilde{q} = (1/s_q)\partial/\partial q$. The component forms of the modified Biot's equations in the complex stretched coordinates are given by

$$\frac{\partial}{\partial t}\begin{bmatrix} \tau_{rr} \\ \tau_{\theta\theta} \\ \tau_{zz} \\ \tau_{rz} \end{bmatrix} = \begin{bmatrix} (H-2\mu)\frac{1+\bar\phi_r}{r} + H(1+\phi_r)\frac{\partial}{\partial r} & (H-2\mu)(1+\phi_z)\frac{\partial}{\partial z} \\ H\frac{1+\bar\phi_r}{r} + (H-2\mu)(1+\phi_r)\frac{\partial}{\partial r} & (H-2\mu)(1+\phi_z)\frac{\partial}{\partial z} \\ (H-2\mu)\left(\frac{1+\bar\phi_r}{r} + (1+\phi_r)\frac{\partial}{\partial r}\right) & H(1+\phi_z)\frac{\partial}{\partial z} \\ \mu(1+\phi_z)\frac{\partial}{\partial z} & \mu(1+\phi_r)\frac{\partial}{\partial r} \end{bmatrix}$$

$$\begin{bmatrix} C\left(\frac{1+\bar\phi_r}{r} + (1+\phi_r)\frac{\partial}{\partial r}\right) & C(1+\phi_z)\frac{\partial}{\partial z} \\ C\left(\frac{1+\bar\phi_r}{r} + (1+\phi_r)\frac{\partial}{\partial r}\right) & C(1+\phi_z)\frac{\partial}{\partial z} \\ C\left(\frac{1+\bar\phi_r}{r} + (1+\phi_r)\frac{\partial}{\partial r}\right) & C(1+\phi_z)\frac{\partial}{\partial z} \\ 0 & 0 \end{bmatrix}\begin{bmatrix} v_{ur} \\ v_{uz} \\ v_{\omega r} \\ v_{\omega z} \end{bmatrix}, \tag{5.1a}$$

$$\frac{\partial p}{\partial t} = -C\left(\frac{1+\bar\phi_r}{r}v_{ur} + (1+\phi_r)\frac{\partial v_{ur}}{\partial r} + (1+\phi_z)\frac{\partial v_{uz}}{\partial z}\right)$$
$$- M\left(\frac{1+\bar\phi_r}{r}v_{\omega r} + (1+\phi_r)\frac{\partial v_{\omega r}}{\partial r} + (1+\phi_z)\frac{\partial v_{\omega z}}{\partial z}\right), \tag{5.1b}$$

$$\left(C_1 + \left(C_2 - \frac{\rho_f^2}{\rho}\right)\frac{\partial}{\partial t}\right)\begin{bmatrix} v_{\omega r} \\ v_{\omega z} \end{bmatrix} = -\begin{bmatrix} (1+\phi_r)\frac{\partial}{\partial r} \\ (1+\phi_z)\frac{\partial}{\partial z} \end{bmatrix} p$$

$$- \frac{\rho_f}{\rho}\begin{bmatrix} (1+\phi_r)\frac{\partial}{\partial r} + \frac{1+\bar{\phi}_r}{r} & -\frac{1+\bar{\phi}_r}{r} & 0 & (1+\phi_z)\frac{\partial}{\partial z} \\ 0 & 0 & (1+\phi_z)\frac{\partial}{\partial z} & (1+\phi_r)\frac{\partial}{\partial r} + \frac{1+\bar{\phi}_r}{r} \end{bmatrix}\begin{bmatrix} \tau_{rr} \\ \tau_{\theta\theta} \\ \tau_{zz} \\ \tau_{rz} \end{bmatrix}, \quad (5.1c)$$

$$\rho\frac{\partial}{\partial t}\begin{bmatrix} v_{ur} \\ v_{uz} \end{bmatrix} = \begin{bmatrix} (1+\phi_r)\frac{\partial}{\partial r} + \frac{1+\bar{\phi}_r}{r} & -\frac{1+\bar{\phi}_r}{r} & 0 & (1+\phi_z)\frac{\partial}{\partial z} \\ 0 & 0 & (1+\phi_z)\frac{\partial}{\partial z} & (1+\phi_r)\frac{\partial}{\partial r} + \frac{1+\bar{\phi}_r}{r} \end{bmatrix}\begin{bmatrix} \tau_{rr} \\ \tau_{\theta\theta} \\ \tau_{zz} \\ \tau_{rz} \end{bmatrix}$$

$$- \frac{\partial}{\partial t}\rho_f\begin{bmatrix} v_{\omega r} \\ v_{\omega z} \end{bmatrix}, \quad (5.1d)$$

where $\phi_q = -\Omega_q e^{-\Omega_q t}*$ $(q=r,z)$ and $\bar{\phi}_r = -\overline{\Omega}_r e^{-\overline{\Omega}_r t}*$ are convolution operators. Eqs. (5.1a)-(5.1d) are the modified Biot's equations in the PML region. These equations automatically reduce to the equations in the computational region, where Ω_q and $\overline{\Omega}_r$ become zero.

Now we discretize the velocities and stresses by using the staggered finite-difference grid as shown in Fig. 1. The grid sizes Δr and Δz in the r- and z-directions, respectively, are constant. All the velocities are temporally discretized at the time points $t=n\Delta t$, while all the stresses are discretized at $t=(n+1/2)\Delta t$. Knowing $v_{ur}, v_{\omega r}, v_{uz}, v_{\omega z}$ at times $t=n\Delta t$, $t=(n-1)\Delta t$, and $\tau_{rr}, \tau_{\theta\theta}, \tau_{zz}, \tau_{rz}, p$ at the time $t=(n-1/2)\Delta t$, the discrete forms of (5.1a) and (5.1b) are used to update $\tau_{rr}, \tau_{\theta\theta}, \tau_{zz}, \tau_{rz}, p$ at time $t=(n+1/2)\Delta t$. For example,

$$\frac{1}{\Delta t}\left(\tau_{rr(j+\frac{1}{2},k+\frac{1}{2})}^{n+\frac{1}{2}} - \tau_{rr(j+\frac{1}{2},k+\frac{1}{2})}^{n-\frac{1}{2}}\right) = \left[(H-2\mu)\left(\frac{v_{ur}^n + Q_{urr}^n}{r} + \frac{\partial v_{uz}^n}{\partial z} + P_{uzz}^n\right) + H\left(\frac{\partial v_{ur}^n}{\partial r} + P_{urr}^n\right)\right.$$
$$\left. + C\left(\frac{v_{\omega r}^n + Q_{\omega rr}^n}{r} + \frac{\partial v_{\omega r}^n}{\partial r} + P_{\omega rr}^n + \frac{\partial v_{\omega z}^n}{\partial z} + P_{\omega zz}^n\right)\right]_{(j+\frac{1}{2},k+\frac{1}{2})}, \quad (5.2a)$$

$$\frac{1}{\Delta t}\left(\tau_{rz(j,k)}^{n+\frac{1}{2}} - \tau_{rz(j,k)}^{n-\frac{1}{2}}\right) = \left[\mu\left(\frac{\partial v_{ur}^n}{\partial z} + P_{urz}^n + \frac{\partial v_{uz}^n}{\partial r} + P_{uzr}^n\right)\right]_{(j,k)}, \quad (5.2b)$$

where $P_{urr}^n, P_{uzz}^n, Q_{urr}^n, P_{\omega rr}^n, P_{\omega zz}^n, Q_{\omega rr}^n, P_{uzr}^n$ and P_{urz}^n denote convolution integrals, for example,

$$P_{urr}^n = -\Omega_r \int_0^{n\Delta t} e^{-\Omega_r(n\Delta t - t)}\frac{\partial v_{ur}(r,z,t)}{\partial r}dt, \quad (5.3a)$$

$$P_{uzz}^n = -\Omega_z \int_0^{n\Delta t} e^{-\Omega_z(n\Delta t - t)}\frac{\partial v_{uz}(r,z,t)}{\partial z}dt, \quad (5.3b)$$

$$Q_{urr}^n = -\overline{\Omega}_r \int_0^{n\Delta t} e^{-\overline{\Omega}_r(n\Delta t - t)}v_{ur}(r,z,t)dt, \quad (5.3c)$$

which can be further approximated with the trapezoidal rule as

$$P_{urr}^n = e^{-\Omega_r\Delta t}P_{urr}^{n-1} - \frac{1}{2}\Omega_r\Delta t\left(e^{-\Omega_r\Delta t}\frac{\partial v_{ur}^{n-1}}{\partial r} + \frac{\partial v_{ur}^n}{\partial r}\right), \quad (5.4a)$$

$$P_{uzz}^n = e^{-\Omega_z\Delta t}P_{uzz}^{n-1} - \frac{1}{2}\Omega_z\Delta t\left(e^{-\Omega_z\Delta t}\frac{\partial v_{uz}^{n-1}}{\partial z} + \frac{\partial v_{uz}^n}{\partial z}\right), \quad (5.4b)$$

$$Q_{urr}^n = e^{-\overline{\Omega}_r\Delta t}Q_{urr}^{n-1} - \frac{1}{2}\overline{\Omega}_r\Delta t\left(e^{-\overline{\Omega}_r\Delta t}v_{ur}^{n-1} + v_{ur}^n\right). \quad (5.4c)$$

The shear modulus μ at the location (j,k) is

$$\mu_{(j,k)} = \left[\frac{1}{4} \left(\mu_{(j-\frac{1}{2},k-\frac{1}{2})}^{-1} + \mu_{(j-\frac{1}{2},k+\frac{1}{2})}^{-1} + \mu_{(j+\frac{1}{2},k-\frac{1}{2})}^{-1} + \mu_{(j+\frac{1}{2},k+\frac{1}{2})}^{-1} \right) \right]^{-1}. \tag{5.5}$$

The formulations to calculate $\tau_{\theta\theta}$, τ_{zz} and p have the similar forms as (5.2a).

Knowing τ_{rr}, $\tau_{\theta\theta}$, τ_{zz}, τ_{rz}, p at times $t = (n-1/2)\Delta t$, $t = (n+1/2)\Delta t$ and $v_{\omega r}$, $v_{\omega z}$ at time $t = n\Delta t$, the discrete expression of (5.1c) is used to update $v_{\omega r}$ and $v_{\omega z}$ at time $t = (n+1)\Delta t$.

$$\left[C_1 \frac{v_{\omega r}^{n+1} + v_{\omega r}^{n-1}}{2} + \left(C_2 - \frac{\rho_f^2}{\rho} \right) \frac{v_{\omega r}^{n+1} - v_{\omega r}^{n-1}}{\Delta t} \right]_{(j,k+\frac{1}{2})} = - \left[\frac{\partial p^{n+\frac{1}{2}}}{\partial r} + P_{pr}^{n+\frac{1}{2}} \right.$$

$$\left. + \frac{\rho_f}{\rho} \left(\frac{\partial \tau_{rr}^{n+\frac{1}{2}}}{\partial r} + P_{rrr}^{n+\frac{1}{2}} + \frac{\tau_{rr}^{n+\frac{1}{2}} + Q_{rrr}^{n+\frac{1}{2}}}{r} - \frac{\tau_{\theta\theta}^{n+\frac{1}{2}} + Q_{\theta\theta r}^{n+\frac{1}{2}}}{r} + \frac{\partial \tau_{rz}^{n+\frac{1}{2}}}{\partial z} + P_{rzz}^{n+\frac{1}{2}} \right) \right]_{(j,k+\frac{1}{2})}, \tag{5.6a}$$

$$\left[C_1 \frac{v_{\omega z}^{n+1} + v_{\omega z}^{n-1}}{2} + \left(C_2 - \frac{\rho_f^2}{\rho} \right) \frac{v_{\omega z}^{n+1} - v_{\omega z}^{n-1}}{\Delta t} \right]_{(j+\frac{1}{2},k)} = - \left[\frac{\partial p^{n+\frac{1}{2}}}{\partial z} + P_{pz}^{n+\frac{1}{2}} \right.$$

$$\left. + \frac{\rho_f}{\rho} \left(\frac{\partial \tau_{zz}^{n+\frac{1}{2}}}{\partial z} + P_{zzz}^{n+\frac{1}{2}} + \frac{\partial \tau_{rz}^{n+\frac{1}{2}}}{\partial r} + P_{rzr}^{n+\frac{1}{2}} + \frac{\tau_{rz}^{n+\frac{1}{2}} + Q_{rzr}^{n+\frac{1}{2}}}{r} \right) \right]_{(j+\frac{1}{2},k)}, \tag{5.6b}$$

where the values of ρ_f, ρ, C_1 and C_2 at the location $(j,k+1/2)$ are the averages of those at the locations $(j-1/2,k+1/2)$ and $(j+1/2,k+1/2)$, while the values at $(j+1/2,k)$ are the averages of those at $(j+1/2,k-1/2)$ and $(j+1/2,k+1/2)$. The variables $P_{pr}^{n+1/2}$, $P_{rrr}^{n+1/2}$, $Q_{rrr}^{n+1/2}$, $Q_{\theta\theta r}^{n+1/2}$, $P_{rzz}^{n+1/2}$ in (5.6a) and $P_{pz}^{n+1/2}$, $P_{zzz}^{n+1/2}$, $P_{rzr}^{n+1/2}$, $Q_{rzr}^{n+1/2}$ in Eq. (5.6b) have the similar forms as (5.4a)-(5.4c).

Then using the calculated $v_{\omega r}$, $v_{\omega z}$ at time $t = (n+1)\Delta t$ and v_{ur}, v_{uz} at time $t = n\Delta t$, the discrete form of (5.1d) is used to update v_{ur} and v_{uz} at time $t = (n+1)\Delta t$.

$$\left[\rho \frac{v_{ur}^{n+1} - v_{ur}^{n-1}}{\Delta t} \right]_{(j,k+\frac{1}{2})} = \left[\frac{\partial \tau_{rr}^{n+\frac{1}{2}}}{\partial r} + P_{rrr}^{n+\frac{1}{2}} + \frac{\tau_{rr}^{n+\frac{1}{2}} + Q_{rrr}^{n+\frac{1}{2}}}{r} - \frac{\tau_{\theta\theta}^{n+\frac{1}{2}} + Q_{\theta\theta r}^{n+\frac{1}{2}}}{r} \right.$$

$$\left. + \frac{\partial \tau_{rz}^{n+\frac{1}{2}}}{\partial z} + P_{rzz}^{n+\frac{1}{2}} \right]_{(j,k+\frac{1}{2})} - \left[\rho_f \frac{v_{\omega r}^{n+1} - v_{\omega r}^{n-1}}{\Delta t} \right]_{(j,k+\frac{1}{2})}, \tag{5.7a}$$

$$\left[\rho \frac{v_{uz}^{n+1} - v_{uz}^{n-1}}{\Delta t} \right]_{(j+\frac{1}{2},k)} = \left[\frac{\partial \tau_{zz}^{n+\frac{1}{2}}}{\partial z} + P_{zzz}^{n+\frac{1}{2}} + \frac{\partial \tau_{rz}^{n+\frac{1}{2}}}{\partial r} + P_{rzr}^{n+\frac{1}{2}} \right.$$

$$\left. + \frac{\tau_{rz}^{n+\frac{1}{2}} + Q_{rzr}^{n+\frac{1}{2}}}{r} \right]_{(j+\frac{1}{2},k)} - \left[\rho_f \frac{v_{\omega z}^{n+1} - v_{\omega z}^{n-1}}{\Delta t} \right]_{(j+\frac{1}{2},k)}. \tag{5.7b}$$

Thus in our scheme the field quantities are discretized in the unified forms in the whole region, including those on any interface in the computational region and those in the PML region.

6 Numerical examples

As an example of using the finite-difference scheme proposed above, we simulate the monopole acoustic logs in fluid-saturated porous formations. For all the simulations in

the following work, the borehole fluid velocity and density are assumed to be 1500m/s and 1000kg/m^3, respectively. A stretching function of $\Omega_q(q) = -V_{max}(a\gamma + b\gamma^2)\ln\beta/T$, $(q = r,z)$ is taken, as given in Wang and Tang [28], where V_{max} is the maximum wave velocity, $\gamma = q/T$, T is the width of the PML, $a = 0.25$, $b = 0.75$ and $\beta = 10^{-6}$ denotes a predefined level of wave absorption. The point source employed is the same as described by Tsang and Rader [26], with the peak pressure being 100Pa at a location of 0.01m away from the source. The source pulse function $s(t)$ used in this paper is

$$s(t) = \begin{cases} \frac{1}{2}\left[1 + \cos\frac{2\pi}{T_c}\left(t - \frac{T_c}{2}\right)\right]\cos 2\pi f_0\left(t - \frac{T_c}{2}\right), & 0 \leq t \leq T_c, \\ 0, & t > 0 \quad \text{or} \quad t > T_c, \end{cases} \qquad (6.1)$$

where f_0 and T_c denote the centre frequency and the pulse width of the source, respectively.

To check the scheme, the finite-difference simulations of the acoustic logs in a homogeneous porous formation are compared with the RAI solutions in Figs. 3 and 4. The parameters of the porous formation are listed in the first column (Formation I) of Table 1. The borehole radius is set to 0.10m.

Table 1: Parameters of the porous formations. The relationships between ϕ and K_b and G_b are assumed to obey the experimental results of Vernik [27].

Parameter	Property	Formation	
		I	II
ϕ	Porosity (%)	20	40
κ_0	Darcy permeability (Darcy)	1	10
K_b	Frame bulk modulus (GPa)	14.39	10.93
G_b	Frame shear modulus (GPa)	13.99	3.01
K_s	Solid bulk modulus (GPa)	35.70	33.17
K_f	Pore fluid bulk modulus (GPa)	2.25	2.0
ρ_s	Solid density (kg/m^3)	2650	2670
ρ_f	Pore fluid density (kg/m^3)	1000	1290
η	Pore fluid viscosity (Pa· s)	10^{-3}	10^{-2}
α_∞	Tortuosity	3	3
m	Dimensionless parameter	8	8

In Fig. 3, the source has a centre frequency and a pulse width of $f_0 = 1$kHz and $T_c = 2.0$ms, respectively. The finite-difference grid sizes are set to $\Delta r = \Delta z = 0.0125$m according to the formula $\Delta r < V_{min}/10f_{max}$ in Alford et al. [1], where V_{min} is the minimum wave velocity, and f_{max} is the maximum source frequency, where $f_{max} = 2f_0$. The time step is chosen as $\Delta t = 2 \times 10^{-3}$ms, following the Courant stability condition $\Delta t < \Delta r/\sqrt{2}V_{max}$. There are 160 and 320 cells respectively in the r- and z- directions of the computational region. The PML contains 40 cells in both directions outside the computational region. Fig. 3(a) gives the comparison of the acoustic pressure full waveforms at different locations along the borehole axis. The waveforms are normalized with respect to the peak
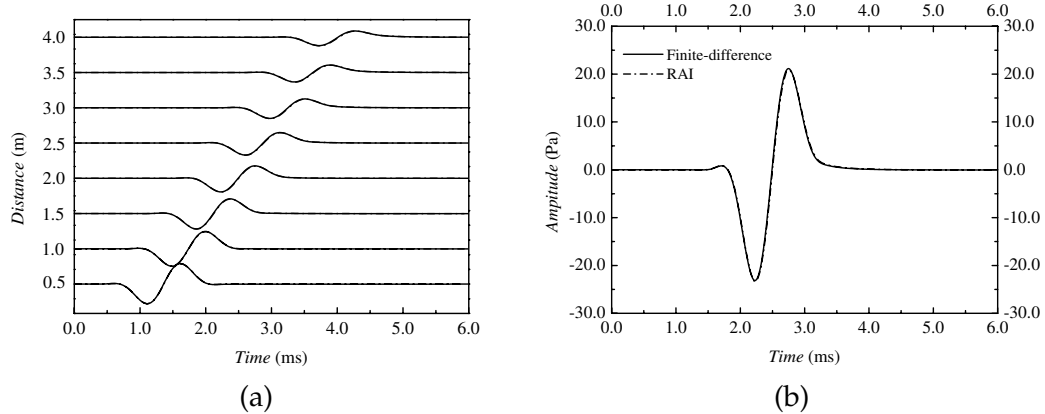
Figure 3: Comparisons between the finite-difference (Solid lines) and the RAI (Dash dot lines) methods of the monopole acoustic logs in a homogeneous porous formation. The centre frequency of the source is $f_0 = 1.0$kHz. (a) Pressure waveforms at different locations along the borehole axis. (b) The waveforms of (a) at the location $z = 2.0$m.
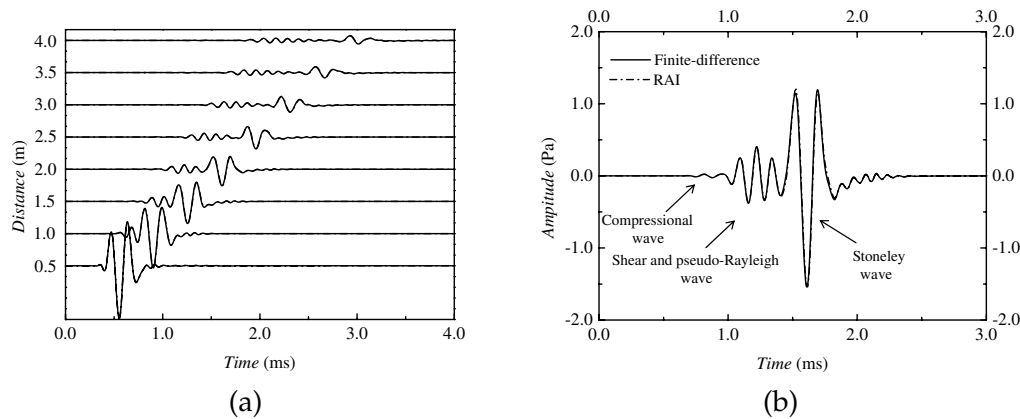

Figure 4: Same as Fig. 3 except that the centre frequency of the source is $f_0 = 6.0$kHz. (a) Pressure waveforms at different locations along the borehole axis. (b) The waveforms of (a) at the location $z = 2.0$m.

value of the response at a location of receiver-to-source distance $z = 0.5$m. More details at $z = 2.0$m are given in Fig. 3(b). At these frequencies, compressional and shear waves are not very well excited, while Stoneley wave dominates the full waveforms. The Stoneley wave attenuation is obvious because the wave energy is gradually leaked into the porous formation by the slow compressional wave. As depicted in Fig. 3, the finite-difference simulations (Solid lines) show excellent agreement with the RAI solutions (Dash dot lines) at different locations from $z = 0.5$m to $z = 4.0$m.

In Fig. 4, the source center frequency and the pulse width are changed to $f_0 = 6$kHz and $T_c = 0.5$ms, respectively. The finite-difference grid sizes are set to $\Delta r = \Delta z = 0.005$m and the time step is chosen as $\Delta t = 8 \times 10^{-4}$ms. Shown in Fig. 4(a) is the comparison of the waveforms at different locations from $z = 0.5$m to $z = 4.0$m. At these frequencies, it is

clear that the full waveforms consist of the compressional wave, the shear and pseudo-Rayleigh wave, and the Stoneley wave. More details at $z = 2.0$m are given in Fig. 4(b). It shows that the phase and the amplitude of the three wave groups agree well between the two methods.

Next the finite-difference scheme is used to simulate the acoustic logs with mud cakes clinging to the borehole wall for investigating the effects of the mud cake on acoustic logs. Shown in Fig. 5 are the acoustic logs at $z = 2.0$m with different mud cake thicknesses being from 0.25cm to 4.0cm. The mud cake is considered as a soft elastic medium between the borehole fluid and the porous formation. The mud cake whose density, bulk and shear moduli are set to 2000kg/m^3, 3.60GPa and 2.16GPa, respectively, has a compressional velocity of 1800m/s and a shear velocity of 1040m/s. The source and the formation parameters are as same as that in Fig. 4. For comparison, the acoustic log without the mud cake is also given in Fig. 5. From the Stoneley wave amplitudes of all the cases provided on the right hand of Fig. 5, it is seen that the amplitude without the mud cake is much less than those with the mud cakes clinging to the borehole wall. The reason is that Stoneley wave generated at the borehole wall is greatly influenced by the wall conditions. When there is no mud cake the borehole wall which is an open pore interface leads to the exchange between the borehole fluid and the pore fluid, thus large wave energy in the borehole is leaked into the formation. For the cases with mud cakes, the sealed pores on the borehole wall which is filled with mud cake block the wave energy into the formation. It is also seen that Stoneley wave amplitude increases with mud cake thickness when the mud cake thickness is less than 1.0cm. Beyond that, the amplitude and the velocity of the Stoneley wave start to decrease because it reflects the characteristics of the mud cake instead of that of the porous formation outside. Fig. 6 is same as Fig. 5 except that the shear modulus of the mud cake decreases five times. The mud cake in Fig. 6 has slower compressional velocity of 1445m/s and shear velocity of 465m/s, having more effect on the acoustic logs than that in Fig. 5. When the mud cake thickness is more than 1.0cm,
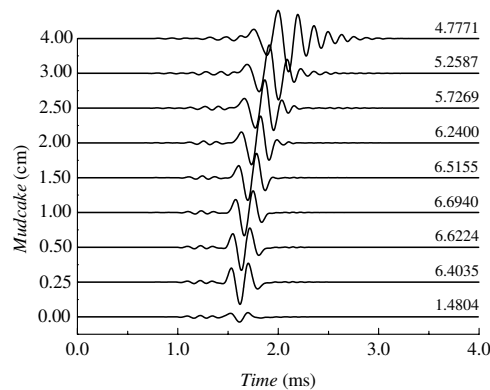

Figure 5: Waveforms of the acoustic logs with different mud cake thicknesses being from 0.25cm to 4.0cm. The source center frequency is $f_0 = 6.0$kHz.
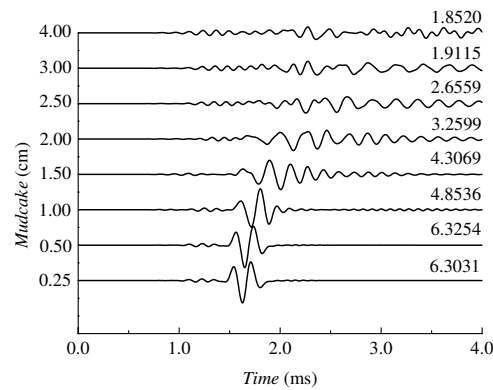
Figure 6: Same as Fig. 5 except that the shear modulus of the mud cake decreases five times.

the waveforms in Fig. 6 become so complex and the amplitude and the velocity of the Stoneley wave decrease more significantly than those in Fig. 5.

Then the acoustic logs in a horizontally stratified porous formation are simulated in Fig. 7. The porous formation around the borehole has three layers, and the medium parameters of the layers are list in Table 1. The layer, which lies between 1.5m and 2.5m above the source, is of Formation II (with higher porosity and permeability). The other two layers are of Formation I. In order to distinguish the reflections of the Stoneley wave at the interfaces between the two layers, the source center frequency and the pulse width are employed as $f_0 = 2$kHz and $T_c = 2.0$ms, respectively. It is clearly shown in Fig. 7 that there are two series of waves reflected respectively from the interfaces at $z = 1.5$m and at $z = 2.5$m. The one from the second interface at $z = 2.5$m is smaller because most of the wave energy is attenuated in the interlayer and transmitted from the interface.

Finally we simulate the acoustic logs in a varying radius borehole embedded in a horizontally stratified porous formation. The formation is the same as in Fig. 7. The
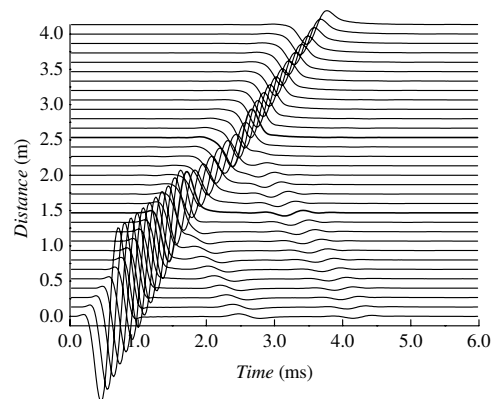

Figure 7: Waveforms of the acoustic logs in a horizontally stratified porous formation. The source center frequency is $f_0 = 2.0$kHz.
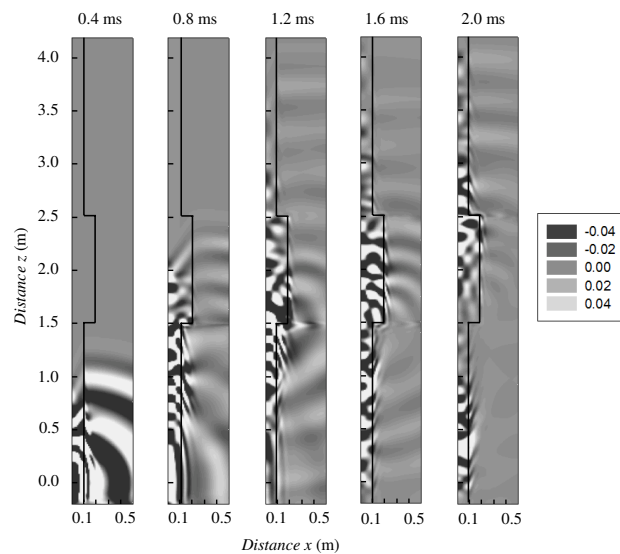
Figure 8: Field distribution of the pressure at five instants of 0.4, 0.8, 1.2, 1.6, and 2.0ms of the acoustic logs in a varying radius borehole embedded in a horizontally stratified porous formation. The source centre frequency is $f_0 = 10$kHz.

borehole radius is set to 0.2m at the range between 1.5m and 2.5m above the source, while it is set to 0.1m at the other locations. In order to identify different wave groups in the wave-field, a higher center frequency $f_0 = 10$kHz and a shorter pulse width $T_c = 0.2$ms are used in this simulation. Fig. 8 shows the wave-field distributions at instants of 0.4, 0.8, 1.2, 1.6, and 2.0ms. The variable borehole radii and the locations of the horizontal interfaces are clearly reflected from the wave-field distributions. In the figure, no obvious wave reflection is observed from the outer boundaries, indicating that the wave-field is well absorbed in the PML. Shown in the first slide at 0.4ms, the fastest pulse in the formation is the transmitted compressional wave from the borehole, and then the pulse with larger amplitude is the transmitted shear wave. The compressional head wave in the borehole can also be seen. In the slide at 0.8ms, the large-amplitude arrival propagates to the interface at $z = 1.5$m, which is the pseudo-Rayleigh wave in the borehole. For the frequency range in this simulation, the Stoneley wave is too weak to be identified within the pseudo-Rayleigh wave packet. In the three later slides at 1.2, 1.6, and 2.0ms, it is seen that part of the pseudo-Rayleigh wave energy in the borehole is reflected back at the interface, and part of the wave energy is leaked into the porous formation by the slow compressional wave and is rapidly dissipated.

7   Conclusions

In this paper, we have validated using the parameter averaging technique to discretize the field quantities on interfaces in finite-difference modeling of elastic waves. On solid-solid and porous-porous interfaces, the discrete equations can be formulated in the forms

of those in the homogeneous media on both sides of the interfaces, if the harmonic mean of shear modulus and the arithmetic means of the other parameters are used. The parameter averaging technique is extended for the interfaces between different kinds of media, such as the solid-fluid, solid-porous, and fluid-porous interfaces.

We have observed that the quantities on a staggered grid must be assigned in this manner that the discontinuous ones are not located on a grid boundary. Once the right staggered grid is used, using the parameter averaging technique to obtain the discrete equations on interfaces is equivalent to deriving from the continuity conditions. The former avoids the additional derivations, thus it takes less computing time and has the advantage of easy treatment of complex interfaces, such as the intersection of three different media.

We have developed a velocity-stress staggered finite-difference scheme for simulating elastic wave propagation in combined structures with solid, fluid and porous subregions. In our scheme, the modified Biot's equations are used to express elastic wave propagation in solid, fluid as well as porous media. Based on the general equations and the parameter averaging technique, the discrete equations have the same forms in the whole computational region including those on any kind of interface that the medium parameters are discontinuous.

We have implemented the 2-D finite-difference scheme in axisymmetric cylindrical coordinates and used it to simulate the acoustic logs in fluid-saturated porous formations. For the case in a homogeneous formation, this algorithm requires three minutes and thirty-six seconds of CPU time, which is four seconds faster than using the previous scheme (Guan et al. [13]). This indicates that the computing efficiency is not reduced when using Biot's equations to express the acoustic fields in the borehole fluid. The finite-difference simulations have been compared with those obtained by the RAI method. The excellent agreement confirms the correctness of the finite-difference scheme. The acoustic logs with a mud cake clinging to the borehole wall have been simulated. The Stoneley wave amplitude without mud cake is much less than those with the mud cakes because the sealed pores block the wave energy into the formation. The Stoneley wave amplitude and velocity are influenced by the thickness and the shear modulus of the mud cake. When the mud cake thickness is more than 1.0cm both the amplitude and the velocity decrease with the increasing thickness, which is more significant for a smaller shear modulus. In a more complex example we simulated the acoustic logs in a varying radius borehole embedded in a horizontally stratified porous formation. Clearly reflected in the simulated wave-field are the variation of the borehole radius and the locations of the horizontal interfaces.

Acknowledgments

References

[1] R. M. Alford, K. R. Kelly, and D. M. Boore, Accuracy of finite-difference modeling of the acoustic wave equation, Geophysics., 39 (1974), 834–842.

[2] J. G. Berryman, and S. R. Pride, Dispersion of waves in porous cylinders with patchy saturation: formulation and torsional waves, J. Acoust. Soc. Am., 117 (2005), 1785–1795.

[3] M. A. Biot, Theory of propagation of elastic waves in a fluid-saturated porous solid, I-low-frequency range, J. Acoust. Soc. Am., 28 (1956), 168–178.

[4] M. A. Biot, Theory of propagation of elastic waves in a fluid-saturated porous solid, II-higher-frequency range, J. Acoust. Soc. Am., 28 (1956), 178–191.

[5] M. A. Biot, Mechanics of deformation and acoustic propagation in porous media, J. Appl. Phys., 33 (1962), 1482–1498.

[6] M. A. Biot, and D. G. Willis, The elastic coefficients of the theory of consolidation, J. Appl. Mech., 24 (1957), 594–601.

[7] C. Boutin, G. Bonnet, and P. Y. Bard, Green functions and associated sources in infinite and stratified poroelastic media, Geophys. J. R. Astr. Soc., 90 (1987), 521–550.

[8] W. C. Chew, and W. H. Weedon, A 3-D perfectly matched medium from modified Maxwell's equations with stretched coordinates, Microw. Opt. Technol. Lett., 7 (1994), 599–604.

[9] N. Dai, A. Vafidis, and E. R. Kanasewich, Wave propagation in heterogeneous, porous media: a velocity-stress, finite-difference method, Geophysics., 60 (1995), 327–340.

[10] H. Deresiewicz, and R. Skalak, On the uniqueness in dynamic poroelasticity, Bull. Seism. Soc. Am., 53 (1963), 783–788.

[11] H. Dong, A. M. Kaynia, C. Madshus, and J. M. Hovern, Sound propagation over layered poro-elastic ground using a finite-difference model, J. Acoust. Soc. Am., 108 (2000), 494–502.

[12] F. Gassmann, *Über die elastizität poröser medien*, Viertel. Naturforsch. Ges. Zürich., 96 (1951), 1–23.

[13] W. Guan, H. Hu, and X. He, Finite-difference modeling of the monopole acoustic logging in a horizontally stratified porous formation, J. Acoust. Soc. Am., 125 (2009), 1942–1950.

[14] D. Ge, and Y. Yan, Finite-Difference Time-Domain Method for Electromagnetic Waves, 2nd edn, XiDian University Press, Xi'an China, 2005.

[15] D. L. Johnson, J. Koplik, and R. Dashen, Theory of dynamic permeability and tortuosity in fluid-saturated porous media, J. Fluid. Mech., 176 (1987), 379–402.

[16] Y. J. Masson, S. R. Pride, and K. T. Nihei, Finite difference modeling of Biot's poroelastic equations at seismic frequencies, J. Geophys. Res., 111 (2006), B10305.

[17] R. Mittet, Free-surface boundary conditions for elastic staggered-grid modeling schemes, Geophysics., 67 (2002), 1616–1623.

[18] A. N. Norris, Radiation from a point source and scattering theory in a fluid-saturated porous solid, J. Acoust. Soc. Am., 77 (1985), 2012–2023.

[19] J. Plona, Observation of a second bulk compressional wave in a porous medium at ultrasonic frequency, Appl. Phys. Lett., 36 (1980), 259–261.

[20] C. J. Randall, Multipole borehole acoustic waveforms: synthetic logs with beds and borehole washouts, Geophysics., 56 (1991), 1757–1769.

[21] J. A. Roden, and S. D. Gedney, Convolution PML (CPML): an efficient FDTD implementation of the CFS-PML for arbitrary media, Micro. Opt. Tech. Lett., 27 (2000), 334–339.

[22] J. H. Rosenbaum, Synthetic microseismograms: logging in porous formations, Geophysics., 39 (1974), 14–32.

[23] D. P. Schmitt, Effects of radial layering when logging in saturated porous formations, J. Acoust. Soc. Am., 84 (1988), 2200–2214.

[24] R. Song, J. Ma, and K. Wang, The application of the nonsplitting perfectly matched layer in numerical modeling of wave propagation in poroelastic media, Appl. Geophys., 2 (2005), 216–222.

[25] R. Song, Parallel Computation of Acoustic Field in Non-Axisymmetric Cased Holes & Theory and Method Studies of Acoustic Cementing Quality Evaluation, Ph.D. Thesis, Jilin University, China, 2008.

[26] L. Tsang, and D. Rader, Numerical evaluation of the transient acoustic waveform due to a point source in a fluid-filled borehole, Geophysics., 44 (1979), 1706–1720.

[27] L. Vernik, Predicting lithology and transport properties from acoustic velocities based on petrophysical classification of siliclastics, Geophysics., 59 (1994), 420–427.

[28] T. Wang, and X. M. Tang, Finite-difference modeling of elastic wave propagation: a nonsplitting perfectly matched layer approach, Geophysics., 68 (2003), 1749–1755.

[29] J. Zhang, Quadrangle-gride velocity-stress finite difference method for poroelastic wave equations, Geophys. J. Int., 139 (1999), 171–182.

[30] Y. Q. Zeng, J. Q. He, and Q. H. Liu, The application of the PML in numerical modeling of wave propagation in poroelastic media, Geophysics., 66 (2001), 1258–1266.

[31] X. Zhu, and G. A. McMechan, Numerical simulation of seismic responses of poroelastic reservoirs using Biot theory, Geophysics., 56 (1991), 328–339.